THE ASTROPHYSICAL JOURNAL, 400:692–698, 1992 December 1


# MEASUREMENT OF THE SOLAR LIMB BRIGHTNESS PROFILE AT 3 MILLIMETERS DURING THE TOTAL ECLIPSE OF 1991 JULY 11

L. BELKORA,[1] G. J. HURFORD, AND DALE E. GARY
Solar Astronomy 264-33, California Institute of Technology, Pasadena, CA 91125

AND

D. P. WOODY
Owens Valley Radio Observatory, California Institute of Technology, P.O. Box 968, Big Pine, CA 93513
*Received 1992 April 27; accepted 1992 June 4*

## ABSTRACT

We observed the solar limb at the point of first contact during the eclipse of 1991 July 11, with a spatial resolution $\sim 1''.6$. The observations were carried out at the Owens Valley Radio Observatory millimeter interferometer, operating at 3 mm (99.46 GHz, with a bandwidth of 350 MHz). The visibility amplitude and phase were modeled to yield the height of the 3 mm limb above the visible photosphere, and the data were differentiated to yield the brightness profile of the limb in strips $\sim 1''.6$ wide. We found that the 3 mm limb extends $7''.5 \pm 0''.8$ or 5500 km above the visible photosphere, with no evidence of a limb spike. This result, and the overall shape of the limb profile, are similar to the interferometric results of Wannier, Hurford, & Seielstad (1983) obtained with the same instrument but without the benefit of an eclipse. The 3 mm limb, at a temperature of $\sim 6500$ K, extends to altitudes far beyond the expected location of the transition region in the model of Vernazza, Avrett, & Loeser (1981). A comparison of the 3 mm profile and an off-band H$\alpha$ photograph of the limb reveals a close correspondence between the 3 mm limb and the height of H$\alpha$ spicules.

*Subject headings:* eclipses — Sun: radio radiation

## 1. INTRODUCTION

On 1991 July 11, during a partial solar eclipse at Owens Valley, we determined the brightness temperature profile of the solar limb at a wavelength of 3 mm (99.46 GHz, $\Delta\nu = 350$ MHz), with $\sim 1''.6$ resolution. High-resolution observations of the solar limb in the millimeter wavelengths are of interest in constructing models of the lower atmosphere. In particular, we seek to elucidate the role of inhomogeneities or features such as spicules, which may dominate the temperature profile at the limb while playing a small role near disk center.

The 3 mm brightness is due to free-free emission from the chromosphere above the temperature minimum region. This belief is based on the density and temperature of the so-called upper chromosphere in semiempirical models such as the VAL (Vernazza, Avrett, & Loeser 1981); even if the vertical scale of the models is uncertain, free-free emission is the most likely because hydrogen ionization sets in at a height of about 1200 km above the visible photosphere and ensures that free-free interactions are the dominant source of opacity for this and higher altitudes, and through the millimeter band. The optical depth of the corona is negligible.

While the emission mechanism pertaining to our observations is well understood, the interplay between atmospheric structures and viewing geometry is not. If the chromosphere were spherically symmetric, uniform, and horizontally stratified, we would see limb brightening for wavelengths above 200 $\mu$m because of the temperature rise with altitude. At 3 mm, smooth-chromosphere models predict not just radial brightening toward the limb but also a limb spike, for as we move off the limb optical depth is provided by material at transition region temperatures. Many previous millimeter and submillimeter studies, however, fail to show the predicted limb brightening or limb spike, and many authors have argued that large-scale or small-scale features introduce such important variations in the temperature and density structure that limb profiles cannot be predicted with models that preserve spherical symmetry and hydrostatic equilibrium (see, for example, Simon & Zirin 1969; Lindsey & Hudson 1976). Here we attempt to identify the features that evidently dominate the brightness temperature profile at the extreme limb.

Section 2 describes the eclipse geometry and our observing procedure. In § 3 we discuss the analysis and results: First we explain what we can learn from the simple record of the occultation as a function of time, and then we derive the brightness profile of the limb averaged over narrow strips in the sky. In § 4 we place our results in the context of other findings in the millimeter and submillimeter bands, and in § 5 we summarize.

## 2. VIEWING GEOMETRY AND OBSERVING PROCEDURES

Figure 1 shows the path of the Moon with respect to the Sun during the eclipse as seen from the Owens Valley Radio Observatory (north is at the top of the figure and west at the right.) The relative size and approximate location of the primary beam of the Owens Valley (OVRO) 10 m dishes is also shown. The interferometer tracked a point 10″ above the photospheric limb during the first contact. Although the eclipse as viewed from Owens Valley was a partial one, so that the motion of the Moon had a nonradial component with respect to Sun center, the motion of the Moon within the beam was predominantly radial and successive intervals of time corresponded to a linear progression of the lunar limb in radial distance. The geometry of the observing conditions was also simplified by the fact that the solar limb has negligible curvature within the 89″ FWHM

[1] Also at the A.P.A.S. Department, University of Colorado, Campus Box 391, Boulder, CO 80309-0391.

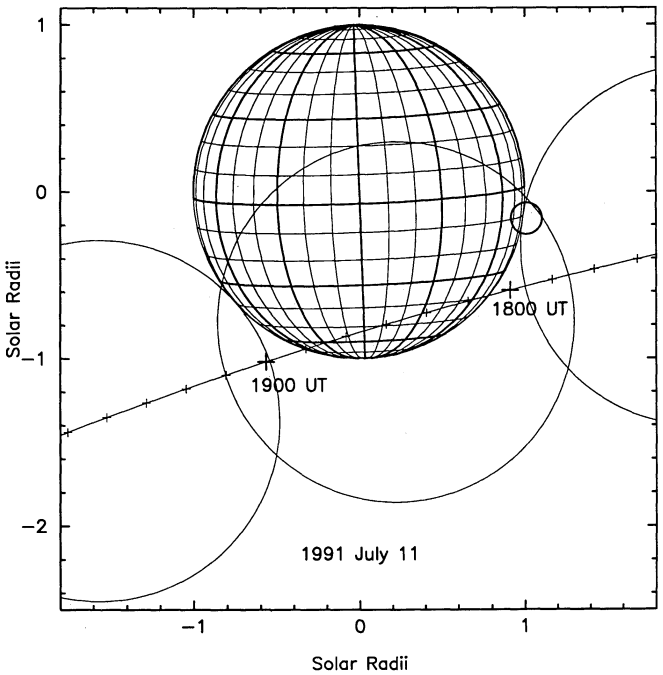


FIG. 1.—Path of the Moon with respect to the Sun during the eclipse (north is at the top of the figure and west to the right). The relative size of the main beam is shown by a circle. The interferometer tracked a point 10″ above the photospheric limb.

size of the main beam. The distance between the limb and the corresponding chord across the field of view was, at worst, 1″, which is about the scale of roughness of the lunar limb due to mountains.

We prepared for the eclipse observations by inserting a 6 dB "Bakelite" absorber in the RF signal path. The calibrator sources 3C 273, Mercury, and Mars were observed through the absorber. We also configured the three antennas of the array to create suitable fringe position angles for observing the first and fourth contacts. The desired fringe position angle is such that the fringes are parallel to the common solar/lunar tangent, as this maximizes the spatial resolution in the radial direction. Furthermore, with this orientation of the fringes the solar source looks like a step function, and the effect of tracking jitter is much less than in the case of single-dish observations; a single dish sees a source with a steep spatial brightness gradient, so that small shifts in pointing have a significant effect on the flux, while the interferometer, insensitive to the large-scale flux in the step function, responds to tracking jitter in a way that is similar to the response to a point source at the center of the beam. For the observation of first contact the angle between the fringes and the solar tangent was only 1°.6, although the main beam took in 5° of arc in position angle along the perimeter of the Sun, so that near the north and south edges of our field of view the angle was 0.9 and 4.1, respectively. The two 10.4 m antennas that formed optimum fringes for first contact were located at 20 m north of the array reference position and 50 m west. At the time of the eclipse the fringe spacing was 13″.5.

We supplemented the OVRO observations with Hα observations made at Big Bear Solar Observatory (BBSO) and used data from the Normal Incidence X-ray Telescope (NIXT), provided by Leon Golub, to judge the coronal activity level around the point of first contact. The NIXT rocket flight occurred only a few minutes before our observations, and from its images we find that the point of first contact is exceptionally quiet, with a low coronal brightness off the limb.

At OVRO, we recorded the visibility amplitude and phase from all three baselines (including the two for which the fringes were not parallel to the solar/lunar tangent) with an integration time of 3.24 s. Some uncertainty was introduced by the fact that transient system errors, such as a loss of phase-lock in one of the receivers, suspended the collection of data. This means that more than 3.24 s of elapsed time was required to obtain 3.24 s of integration time. We have no way to identify the period or periods during the sample interval when the 3.24 s of integration occurred. To understand the effect of the noncontinuous integration, we worked with two versions of the data (later folded together), one in which the assignment of a time to a sample was based on the assumption that all the integration occurred at the beginning of the sample interval, and the other, the end of the sample interval. Since the flux generally decreased with time as the occultation progressed, the assumption that all the integration occurred at the beginning of the sample interval tends to underestimate the flux at the assigned time, while the assumption that all the integration occurred at the end tends to overestimate the flux. The two versions of the data, which we call "early-sampled" and "late-sampled," thus represent the two extreme cases, which determine the amplitude errors indicated on our plots.

The spatial resolution was degraded by the extra long sampling intervals, regardless of the fact that the total length of *integration* was always 3.24 s. During the course of our observation the Moon moved at a rate of 0″.40 $s^{-1}$, so the resolution, based on the best sample interval of 3.24 s, is 1″.3. The spatial resolution that pertains around the time of first contact is about 1″.6 and certain portions of the disk were seen with a resolution of 2″.7. These variations complicated our analysis, but even in the worst case our resolution was better than has been obtained with previous observations near the same wavelength.

We will show in the analysis that the most significant source of uncertainty in our limb profiles is due not to the errant integration times but to atmospheric fluctuations and receiver noise.

## 3. ANALYSIS AND RESULTS

### 3.1. *The Occultation Record*

Figure 2 (*top and bottom panels*) shows the visibility amplitude and phase of the occultation record. We emphasize for clarity that the plot shows correlated amplitude, not total power. The interferometer phase, shown in the bottom plot, generally acts as a position indicator for the dominant source in the field of view; in this case, the interferometer tracked a fixed point near the solar limb, and the initial phase represents the position of the sharp fall-off in the limb brightness. As the moon occults the solar limb, the sharpest fall-off in brightness occurs at the lunar limb so the phase changes to reflect the changing position of the lunar limb.

The behavior of the amplitudes and phases can thus be summarized as follows. In the precontact period (to the left in the figure) the amplitudes and phases are roughly constant. When the Moon first occults a portion of the extended solar limb, near $17^h15^m40^s$ UT, we see what may be a small dip in the amplitude followed by a rise above the precontact level. The phase appears constant around this time. Thereafter the flux

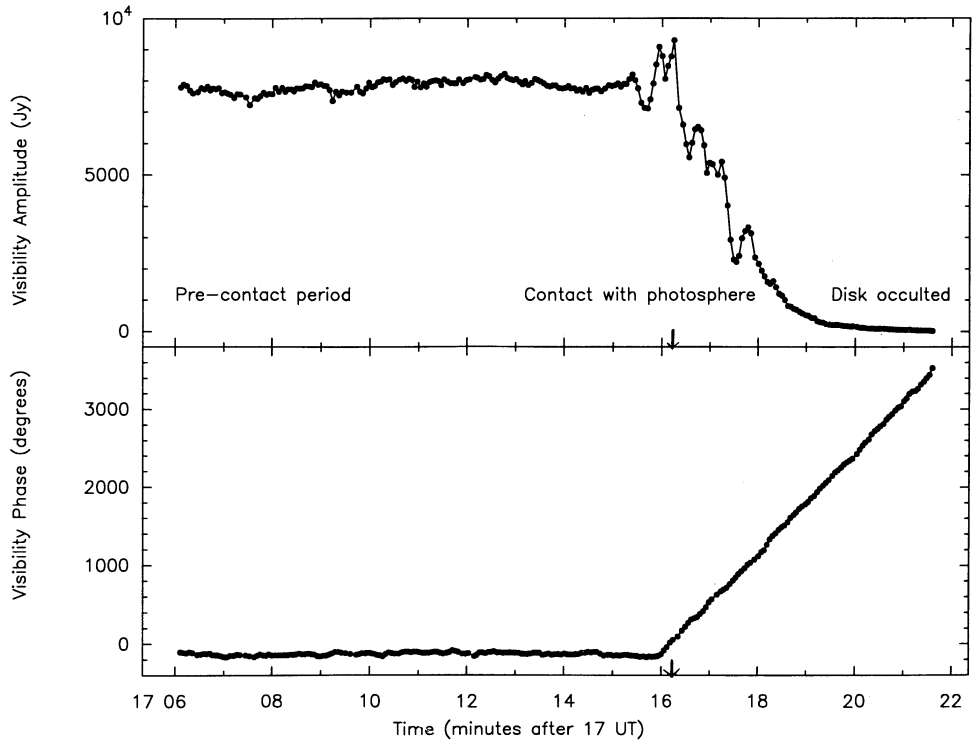


FIG. 2.—Amplitude (*top panel*) and phase (*bottom panel*) of the visibility around the time of first contact, for a baseline with fringes parallel to the limbs. The behavior of each is explained in the text. The arrows point to the time at which the photosphere was occulted.

level drops in proportion to the decreasing area of exposed disk in the beam, except that there are "bumps" and "dips" superposed on the curve. The phases ramp linearly as the Moon traverses the fringes nearly perpendicularly.

The "bumps and dips" in the occultation record are not to be confused with the pattern of oscillations seen in single-dish lunar occultation observations (lunar occultation as a special form of interferometry is described by Thompson, Moran, & Swenson 1986). This latter pattern is due to Fresnel or near-field diffraction around the Moon of plane waves from the Sun, and the varying amplitude of the oscillations comes from the covering-up of varying orders of Fresnel zones by the Moon. Fresnel diffraction is not relevant to our observations because at $\lambda = 3$ mm the width of the first Fresnel zone is only 0".42, and our resolution is at least 3 times this width. We investigated the possibility of some residual effect of Fresnel diffraction and, in our modeling, found no significant effect.

To show how the occultation record comes about we create a model of the eclipse. Figure 3 (*top panel*) shows a model of the solar limb which consists of a step function convolved with a Gaussian, 3" wide, centered 8" above the photosphere—similar to the limb found by Wannier, Hurford, & Seielstad (1983)—and multiplied by a Gaussian beam of width 89", centered 10" above the photosphere. The middle and bottom panels show that resulting visibility amplitude and phase as a function of time as would be measured by our interferometer, for a step function lunar limb occulting the model of the top panel from left to right. The precontact visibility amplitude reflects the spacing of the interferometer and the smoothness of the effective solar profile at the scales the interferometer is sensitive to. The rise in the visibility at contact occurs because the Moon sharply cuts off the solar limb profile and boosts the high spatial frequencies in the Fourier transform of the resulting profile. The small dip seen in the data just prior to the rise can be reproduced with limb models (not shown) that have a broad "tail" with a small step in it.

The height of the 3 mm limb above the photosphere can be found directly from the occultation record by comparing the observed time of first contact with the time at which the Moon was due to occult the photosphere. Calculations for the OVRO site obtained from the US Naval Observatory (courtesy of A. D. Fiala, Nautical Almanac Office) as well as our own calculations based on their ephemeris show that the lunar limb began to occult the photosphere at 17:16:12.9 UT. We found the observed time of first contact in our record from the behavior of the visibility phase, which is simpler to interpret than the fluctuations in the amplitude. We constructed a model of the phase as a function of time in which the slope was determined using the emphemeris to calculate the relative position of the Moon in the fringe pattern. The precontact phase for the model was adopted from the observed, immediate precontact phase in the data. We shifted the model in time with respect to the data, interpolated the model to the data sample times, and searched for the minimum displacement between the two curves. The time corresponding to this minimum difference was then taken as the observed first contact time.

The observed first contact time occurred significantly before the predicted photospheric first-contact time. The "early-sampled" data (see § 2) give a first-contact time corresponding to a distance of 7".6 above the photosphere, while the "late-sampled" data give 7".3, well within half of a resolution element (1".6 given by the time between samples) so we adopt the value 7".5 $\pm$ 0".8 for the observed height of the solar limb. We note that the fit was marginally better for the "early" version and

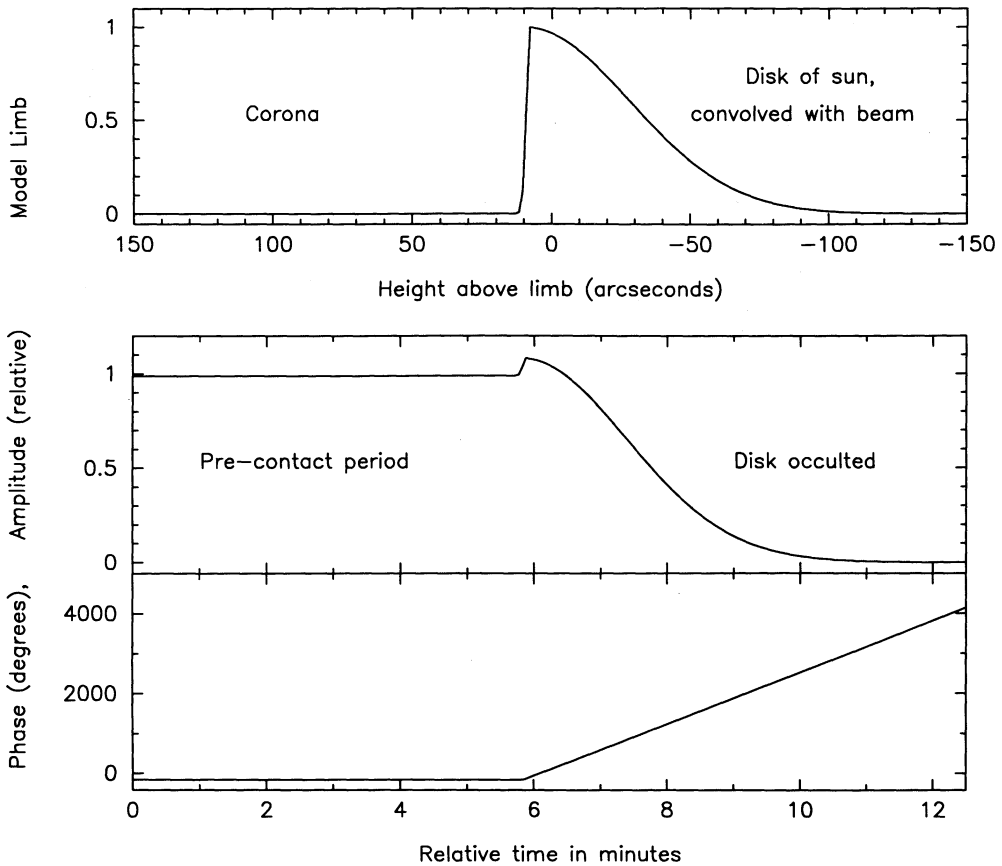


FIG. 3.—*Top panel:* Model of the solar limb consisting of a step function centered 8″ above the photosphere, convolved with a Gaussian 3″ wide, and multiplied by a Gaussian beam of width 89″ centered 10″ above the photosphere. *Middle panel:* Amplitude of the visibility as a function of time, as would be measured by our interferometer, for a step function limb occulting from left to right in the model of the top panel. *Bottom panel:* Corresponding visibility phase.

will indicate one or two data points in the final limb profile where the earlier points appear to be more trustworthy.

The height measured by our technique is a lower limit to the 3 mm limb and turns out to be about the half-power point of the brightness profile (as will be shown in § 3.2). Any extended "tail" in the profile could not be seen directly in the phases due to noise. Some variation can be seen in the amplitudes prior to the ramp-up in phases; as will be seen in § 3.2, this corresponds to a bump in the brightness profile which occurred far above the half-power point of the limb. This feature has a low standard deviation above the mean of the precontact values and could be due to a region over the limb. The Solar Geophysical Data reports indicate that on the previous day, July 10, NOAA region 6706 (a small, rapidly decaying region) was at S 10, W 75, which puts it on the west limb on July 11. However, the NIXT image of this location showed an exceptionally quiet limb in soft X-rays, so the reality of the feature remains questionable.

### 3.2. *The Strip Brightness Profile*

Following Gary & Hurford (1987), we perform a vector subtraction of the visibility at time $t_n$ from the visibility sample for $t_{n+1}$, to convert the time profile in Figure 2 to the strip brightness profile of the solar limb. Assuming no time-varying sources are present, this gives the visibility of the strip occulted in the intervening time. In applying this procedure to our data we first linearly interpolate the "early-sampled" and "late-sampled" versions of the occultation record so that the data points occur at regular intervals of 1.8 s, which is half the mean sample interval, so that the strips on the sky have equal width. In the final result, we will remove this oversampling by using a three-point running mean.

The amplitude of the vector difference of the data in Figure 2 is plotted in the top panel of Figure 4. A high level of fluctuations is apparent in this figure, even in the precontact period when no fluctuations are expected at all. When the precontact amplitudes and phases are plotted on a polar plot, the variations are found to be mostly in the phases, probably primarily due to the atmosphere.

Because of the unusual amount of phase noise, we searched for an alternate treatment of the data that would be less sensitive to the phases. One option is to ignore the phases completely and rely on our knowledge of the geometry of the eclipse, which is very precise; we demonstrated in § 3.1 that the phase for the occultation of a uniform solar disk can be predicted very accurately. We expect that deviations from a uniform solar disk will appear about equally in the amplitudes and phases, so by substituting model phases, we reduce our sensitivity to these deviations, but will have less uncertainty than when using the noisy phases. Figure 4 (*bottom panel*) shows the dramatic reduction in the noise level when the "early" difference plot is calculated with model phases.

The substitution of model phases must be done carefully because computer modeling shows that the visibility phases

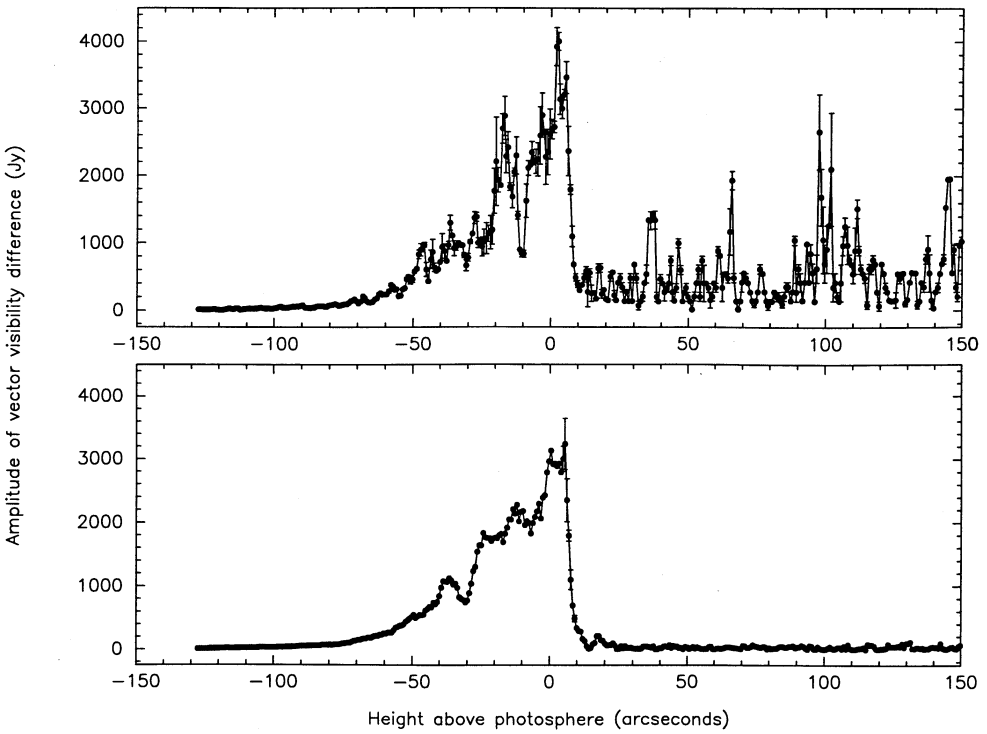


FIG. 4.—*Top panel:* Amplitude of the vector difference of the visibilities in Fig. 2, computed as described in the text. *Bottom panel:* Same as top panel, except that phases computed from the emphemeris have been substituted for the measured phases. The error bars show the amplitude range when the "early" and "late" data are used, as explained in the text.

that pertain to the occultation of realistic limb profiles do not start to wind or ramp up linearly at the time of first contact. They may, for complex or extended limb profiles, show a dip or a gradual change in slope, and this has a significant effect on the shape of the derived limb profile. Accordingly, we substituted artificial phases for real ones in our data, except for the five or six points that defined the onset of the phase wind.

Each point in the vector difference profile, such as shown in Figure 4 using the model phases, represents the total flux of a strip of the exposed Sun within the primary beam. The effect of the primary beam is to reduce the flux near the edge of the beam, as is easily seen at the left-hand side of the profile in Figure 4. We can convert the flux from each strip into a one-dimensional brightness temperature using the effective area of the strip at each time, under the assumption that the brightness temperature is uniform along the strip except for the effect of the primary beam. Figure 5 shows the data converted to brightness temperature, and smoothed with a three-point running mean to remove the oversampling we introduced when we linearly interpolated the data at half the mean sample interval. We have confidence in the correction for the primary beam out to the half-power points and display only that spatial extent in the figure.

The limb profile of Figure 5 displays several important features. The mean brightness temperature on the outer 20″ of the disk is about 6300 K, in agreement with the 3.0 and 3.09 mm values given by Linsky (1973) and in accord with the VAL model temperature some distance above the temperature minimum. From the photosphere to a height of ~5″.5 (4100 km) the temperature stays within the range measured on the disk, then it falls precipitously to about 1500 K in the next 3″. After this, the decrease is more gradual until at ~12″ above the photosphere the form of the profile is lost in noise. The half-maximum point is at an altitude of about 7″.4, which is essentially the same height we obtained from the behavior of the phases alone in the occultation record. The root mean square temperature of about 100 K in the precontact period is a lower limit, but reasonable approximation, to the noise level. The error bars reflect the difference between the "early-sampled" and "late-sampled" versions of the data; if we lean more toward the "early-sampled," as discussed in § 3.1, the only difference worth noting is that the point about 5″.5 above the photosphere is likely to fall at the bottom of the error bar, making a smoother connection with the rest of the profile.

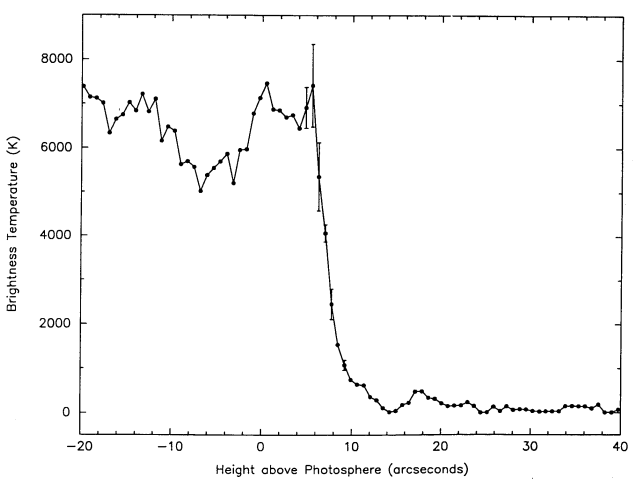


FIG. 5.—The limb profile, derived using the ephemeris phases. The attenuation due to the primary beam has been removed.

As we have already indicated, the profile we obtain does not show a uniform brightness temperature on the disk. Seven arcseconds inside the photosphere, the brightness temperature is down by almost 30%; then it rises again. Some of this nonuniformity is probably due to noise in the data, but the broad features affecting many samples are probably due to real brightness temperature variations. Full disk observations near 3 mm with spatial resolution of about 1′ show amplitude variations of ~20% due to active regions and filaments (Hurford 1986). If the variations in Figure 5 are real, they could be due to plage elements or other bright or dark features on the disk, on a scale that is difficult to see on optical photographs because the region is so close to the limb and is therefore severely foreshortened.

## 4. DISCUSSION

Our detection of photospheric-temperature plasma at an altitude of 5500 km above the visible photosphere complements data from a wide spectral range in demonstrating the inadequacy of certain models—those that depict the chromosphere as smooth and that ignore spicules and other features not in hydrostatic equilibrium. A survey of the literature reveals that in the range from 30 $\mu$m to 3 mm the data display two types of phenomena that the authors surveyed cannot accommodate with hydrostatic models. The phenomena are, first, the existence of millimeter opacity at heights well above the visible photosphere, i.e., the extension of the limb beyond the photospheric radius, and, second, the absence (in almost all cases) of a limb "spike" or transient. In the range 100 $\mu$m to 1 mm, some single-dish data suggest that large-scale limb brightening is suppressed by inhomogeneity in the chromosphere, adding to the list of phenomena that cannot be accommodated, but these data suffer from the uncertainty of beam deconvolution, and we will not comment further on the limb brightening question.

We illustrate the difficulty of reconciling the data and the hydrostatic models by considering the predictions of the VAL at 3 mm. By our reckoning the VAL model predicts, at this wavelength, a limb spike of $T_B \sim 25{,}000$ K about 3″ above the limb. The temperature is indicative of the transition region, which in this model occurs near 2200 km. The density along the line of sight is high enough to provide unit optical depth when the line of sight intersects points below 3″ or ~2200 km altitude; above this, the plasma becomes optically very thin and the brightness temperature drops rapidly. There should be no significant emission above ~3000 km. The measured extensions, on the other hand, strongly suggest the presence of cool ($\leq$10,000 K), dense material above 5000 km. Labrum, Archer, & Smith, in an admirable 1978 paper, were perhaps the first with resolution comparable to ours to report on the 3 mm radio limb explicitly, and they found an extension of $5600 \pm 800$ km. The other observations near 3 mm with resolution of a few arcseconds are those at 2.7 mm by Wannier et al. (1983), who determined a limb extension in accord with ours, and those at 3.5 mm of White & Kundu (1992), who observed the 1991 July eclipse with the Berkeley-Illinois-Maryland array and found a limb extension of about 11″. All of these authors found the limb to be free of spikes. Perhaps even more difficult to reconcile with the hydrostatic models are the interferometric data at 1.3 mm of Horne et al. (1981): They found a limb extension of 8″.1, similar to ours at 3 mm, whereas the difference in observing wavelength should have led, in the case of a hydrostatic model, to their finding a much smaller limb extension.

The cool, dense material we infer from the limb extensions could be present *in addition to* the material described by the VAL, if it were structured in such a way as to be more visible at the limb than on the disk. In this case the denser material would provide most of the opacity and would effectively obscure the hot, less dense matter. In such a two-component model, it is tempting to associate the obscuring component with spicules. Spicules are rather sparsely distributed when one views the disk of the Sun, but at the limb, spicules over a wide range of longitudes project densely against the sky to form an edge approximately 5000 kilometers above the photosphere. We are not the first to suggest that spicules provide the opacity to extend the radio limb above the photosphere; Coates (1958) did so in a remarkable early study, and the models of Thomas & Athay (1961, see chap. 8) and Lantos & Kundu (1972) are similar in general terms. However, our high-resolution profile does permit us to compare the 3 mm and optical limbs directly. When we overlay our one-dimensional brightness profile on an off-band Hα image, as in Figure 6, we find that the sharp edge of the 3 mm profile lies very close to the edge of spicules.

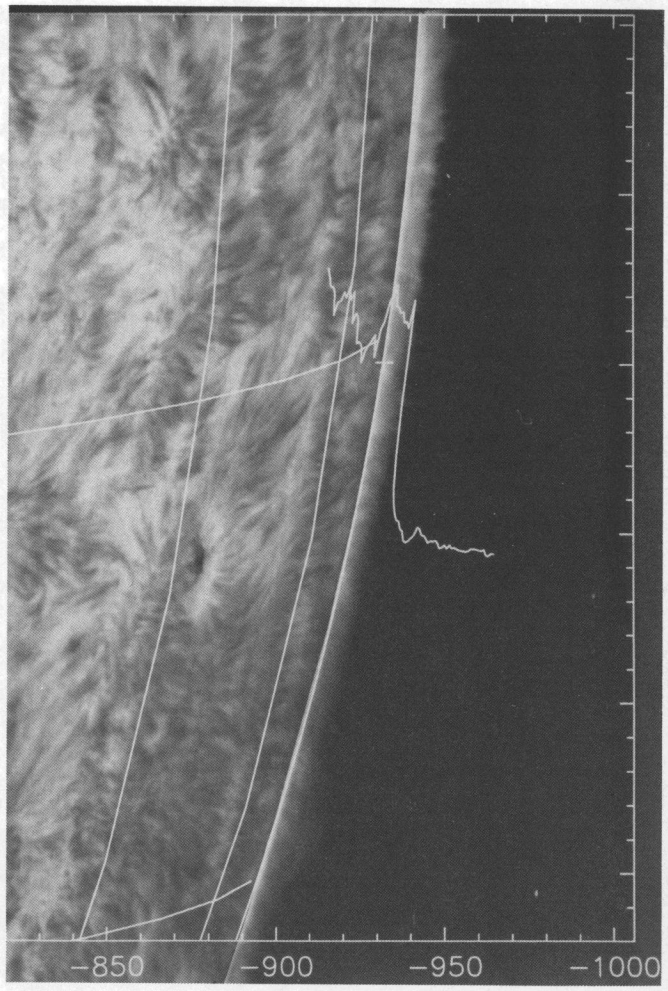


FIG. 6.—Off-band Hα photograph of the region near the limb, taken at BBSO on the day of the eclipse, overlaid with solar latitude and longitude lines at 10° intervals and with a plot of the 3 mm limb profile. *The vertical scale of the radio profile is arbitrary.* The plus sign shows the center of the beam. The spicules can be seen as a fuzzy edge above the optical limb, nearly at the same height as the sharp cutoff in the radio profile. The contrast of the Hα spicules was photographically enhanced for clarity.

The sharp edge in the radio profile probably corresponds to $\tau = 1$, in which case the relatively flat part of the limb profile is optically thick and the temperature of spicule material is only about 6000 K. A crude calculation of the electron density at the altitude corresponding to the edge in the 3 mm profile, assuming free-free opacity, gives $\sim 10^{11}$ cm$^{-3}$.

## 5. SUMMARY

We found that at 3 mm the solar limb extends $7''.5 \pm 0''.8$ or 5500 km above the visible photosphere, as measured by the onset of the ramp-up in the visibility phases. The limb profile is relatively steep at this height, so the measurement of the limb extension according to the half-power point rather than the phase wind gives essentially the same result. Our data do not give information on the center-to-limb brightness profile; we have confidence in the brightness temperature only to 20″ inside the limb, as this represents the half-power point of the primary beam. We can say, however, that the disk brightness temperature at the extreme limb appears to be affected by features that vary in amplitude by about 30% over about 5″, and there is no underlying trend of limb brightening or darkening that we can detect.

The data of Wannier et al. (1983), with which ours basically agree, were taken with the same interferometer at Owens Valley but without the benefit of an eclipse and with resolution of about 6″. They determined a best-fit limb profile that is very similar to ours, with a shallow decline above the limb, then a "knee" and a steeper drop in brightness temperature (see Fig. 4 in their paper). The main difference is a larger limb extension of 8″–12″. The variability of the limb extension may be a real solar effect or of instrumental origin, but in any case we believe that their results can be reconciled with ours by taking into consideration the difference in spatial resolution and the difference in the way the extension was measured.

Besides the results of Wannier et al. (1983), we find consistency only with the single-dish measurement of Labrum et al. (1978), and with the interferometric data of White & Kundu (1992), notwithstanding the diversity of published limb profiles near $\lambda 3$ mm. Most of the limb information obtained to date comes from single-dish observations, and it seems likely that their inconsistency stems from poor spatial resolution and from the difficulty of deconvolving the beam profile. The interferometric data of White & Kundu (1992) at 3.5 mm are of special interest because they pertain to the same eclipse, and very nearly the same limb. Using the same definition we used in § 3.1, the onset of phase wind in the occultation record, they find a limb extension of 11″, similar to, but significantly different from, our measurement of $7''.5 \pm 0''.8$. Nor can the discrepancy be completely attributed to the 15% difference in observing frequency, since the White et al. observations at 86 and 89 GHz show no difference in onset times. The true test of the discrepancy will come when a vector-difference profile is obtained from the White et al. data, and the two limb profiles are compared over their entire heights.

In the meantime, the high spatial resolution of our limb profile has allowed us to compare the 3 mm limb with that in off-band H$\alpha$ in Figure 6, and we find that the sharp edge of the 3 mm profile corresponds quite closely to the apparent top edge of the spicules. This supports our hypothesis that spicules consist of relatively cool ($\sim$6000 K) material capable of obscuring any transition-region type gas at altitudes up to at least 3500 km.

We thank G. Dulk and M. W. Ewell for valuable discussions and N. Scoville for facilitating our use of the millimeter array at Owens Valley. We thank the referee, R. G. Athay, for his careful, valuable criticism. This work was funded in part by NSF grants ATM-9013173 and AST-8919770 and by NASA under grant NAGW-3005 to the California Institute of Technology and under grant NAGW-1994 to the University of Colorado.

## REFERENCES

Coates, R. J. 1958, ApJ, 128, 83
Gary, D. E., & Hurford, G. J. 1987, ApJ, 317, 522
Horne, K., Hurford, G. J., Zirin, H., & De Graauw, T. 1981, ApJ, 244, 340
Hurford, G. J. 1986, in Solar Flares and Coronal Physics Using P/OF as a Research Tool, ed. E. Tandberg-Hanssen, R. M. Wilson, & H. S. Hudson (NASA CP-2421), 191
Lambrum, N. R., Archer, J. W., & Smith, C. J. 1978, Sol. Phys., 59, 331
Lantos, P., & Kundu, M. R. 1972, A&A, 21, 119
Lindsey, C., & Hudson, H. S. 1976, ApJ, 203, 753
Linsky, J. L. 1973, Sol. Phys., 28, 409
Simon, M., & Zirin, H. 1969, Sol. Phys., 9, 317
Thomas, R. N., & Athay, R. G. 1961, Physics of the Solar Chromosphere (New York: Interscience)
Thompson, A. R., Moran, J. M., & Swenson, G. W., Jr. 1986, Interferometry and Synthesis in Radio Astronomy (New York: John Wiley and Sons)
Vernazza, J., Avrett, E., & Loeser, R. 1981, ApJS, 45, 635
Wannier, P. G., Hurford, G. J., & Seielstad, G. A. 1983, ApJ, 264, 660
White, S. M., & Kundu, M. R. 1992, in IAU Symp. 154, Infrared Solar Physics, ed. D. M. Rabin & J. T. Jeffries (Dordrecht: Kluwer)